

Effects of non-integrability in a non-Hermitian time crystal

Weihua Xie* and Michael Kolodrubetz†

Department of Physics, The University of Texas at Dallas, Richardson, Texas 75080, USA

Vadim Oganesyan‡

Physics Program and Initiative for the Theoretical Sciences,

The Graduate Center, CUNY, New York, New York 10016, USA and

Department of Physics and Astronomy, College of Staten Island, CUNY, Staten Island, New York 10314, USA

Daniel P. Arovas§

Department of Physics, University of California at San Diego, La Jolla, California 92093, USA

(Dated: December 6, 2024)

Time crystals are systems that spontaneously break time-translation symmetry, exhibiting repeating patterns in time. Recent work has shown that non-Hermitian Floquet systems can host a time crystalline phase with quasi-long-range order. In this work, we investigate the effect of introducing a non-integrable interaction term into this non-Hermitian time crystal model. Using a combination of numerical TEBD simulations, mean-field analysis, and perturbation theory, we find that the interaction term has two notable effects. First, it induces a shift in the phase diagram, moving the boundaries between different phases. Second, a sufficiently strong interaction induces an unexpected symmetry-breaking transition, which is not captured by the mean-field approach. Within average Hamiltonian theory, we trace this back to a ferromagnetic transition in the anisotropic non-Hermitian XXZ model. Our results demonstrate that the interplay between non-Hermitian dynamics and many-body interactions can lead to novel symmetry breaking.

I. INTRODUCTION

Real-life quantum systems invariably interact with their environment, leading to non-unitary dynamics. These interactions are often modeled using the Lindblad formalism [1]. When focusing on trajectories without quantum jumps, the corresponding dynamics can be described by a non-Hermitian Hamiltonian [2]. Non-Hermitian systems reveal distinct characteristics such as unconventional band topology [3], skin effects [4], and exceptional points [5–7], along with various other phenomena [8–12]. Increasingly, experimental setups are capable of accessing non-Hermitian regimes, thus enabling the observation of these phenomena in practice [13–17]. Furthermore, it was more recently found by some of us that non-Hermitian dynamics opens the door to more interesting forms of time crystals [18]. More broadly, [18] suggests that the canonical works by Lee and Yang, M.E. Fisher, Wu, Griffiths, and others on statistical mechanics at complex temperature (cf. [19–21]) may be reinterpreted as non-Hermitian quantum circuits. Therefore, it seems likely that non-Hermitian Hamiltonians may have more complicated properties than Hermitian systems, which are inherited from equilibrium statistical mechanics.

One of the phases found in Basu *et al.* [18] is a time crystal with quasi-long-range order in time, which differs

from time crystals that are found in more conventional Hermitian systems. Time crystals – systems that spontaneously break time-translation symmetry (TTS) to form repeating patterns in time – were originally proposed by Wilczek for static Hamiltonians [22], but such breaking of continuous time-translation symmetry was later found to be impossible [23]. However, the field was revived by the discovery that discrete time-translation symmetry can be broken, leading to the realization of time crystals through periodic (Floquet) driving [17, 24–30]. The non-Hermitian time crystal from [18] falls somewhere between these two classes, as it involves Floquet drive but exhibits TTS-breaking with continuously tunable period. The non-Hermitian nature of the model allows this possibility, falling outside of the conditions for the no-go theorem [23].

In this work, we consider extending the non-Hermitian time crystal from Basu *et al.* [18] by adding a transverse interaction between the Ising spins, which is known to break integrability. This allows us to probe the stability of the non-Hermitian time crystal, which is unclear for most driven non-Hermitian systems. On the one hand, non-Hermitian dynamics allows flow to a unique steady state, which is morally similar to a ground state and therefore is expected to be stable to weak integrability-breaking. On the other hand, the model of interest is a (non-Hermitian) Floquet system, and integrability-breaking generally leads to heating in Floquet systems which usually kills phases of matter like time crystals. Assessing this competition in the non-Hermitian time crystal is a key point of this paper.

The remainder of this paper proceeds as follows. In section II, we describe the non-Hermitian Floquet-

* wx180002@utdallas.edu

† mkolodru@utdallas.edu

‡ vadim.oganesyan@csi.cuny.edu

§ arovas@physics.ucsd.edu

Ising model, the non-integrable interaction term, and the methods that we use to simulate its dynamics using time-evolving block decimation (TEBD). In section III, we present TEBD data suggesting a shift in the phase diagram induced by interactions as well as a novel symmetry-breaking within the time-crystalline phase. We employ a mean-field treatment to analytically verify this shift and use average Hamiltonian theory to explain the additional symmetry breaking. Finally, in section IV, we conclude with a discussion of generality of these results.

II. MODEL

Consider the two-dimensional classical Ising model:

$$H = - \sum_{i,j} (J_x Z_{i,j} Z_{i+1,j} + J_y Z_{i,j} Z_{i,j+1}) \quad (1)$$

where $Z_{i,j}$ are Pauli operators living on a square lattice. The conventional classical-to-quantum mapping takes the 2D classical Ising model at finite temperature to a one-dimensional Hermitian quantum Ising model [31]. Ref. [18] considered what happens for complex temperature, which has separately studied in the theory of phase transitions as it enables zeros of the partition function, known as Lee-Yang zeros [19, 20]. However, [18] proceeded by noting that complex temperature can also be considered as maps the classical 2D Ising model to a non-Hermitian quantum circuit, namely a non-Hermitian Floquet version of the transverse-field Ising model in which each Floquet cycle consists of first applying the bond terms and then applying the field terms:

$$\begin{aligned} \mathcal{W} &= W_{1,2} W_{2,3} \cdots W_{L-1,L} = \exp \left(J \sum_{j=1}^{L-1} Z_j Z_{j+1} \right) \\ \mathcal{V} &= V_1 V_2 \cdots V_L = \exp \left(\gamma \sum_{j=1}^L X_j \right), \end{aligned} \quad (2)$$

with a non-unitary cycle evolution operator $\mathcal{U} = \mathcal{V}\mathcal{W}$. The parameters are defined through the complex-temperature Ising mapping as $J = \beta J_y$ and $\tanh \gamma = \exp(-2\beta J_x)$ with parameters chosen to be anisotropic: $J_x = 1$ and $J_y = 0.1$. In the thermodynamic limit, $L \rightarrow \infty$, this system has multiple steady state phases (see Fig. 1), including paramagnet, ferromagnet, and time crystal (NFM1 phase) [18]. The time crystal, in particular, emerges due to a degeneracy in the decay rates of two single-particle (Majorana) modes at momenta $\pm k^*$. Linearizing around these points leads to a Fermi surface-like dispersion for the imaginary part of the energy, resulting in a power-law decay of 2-time correlation functions.

The time-crystalline phase is described by the two-time correlation function

$$C(N) = \langle Z_{j'}(N) Z_j(0) \rangle = \frac{\text{Tr}[Z_{j'} \mathcal{U}^N Z_j \rho_0 (\mathcal{U}^\dagger)^N]}{\text{Tr}[\mathcal{U}^N \rho_0 (\mathcal{U}^\dagger)^N]} \quad (3)$$

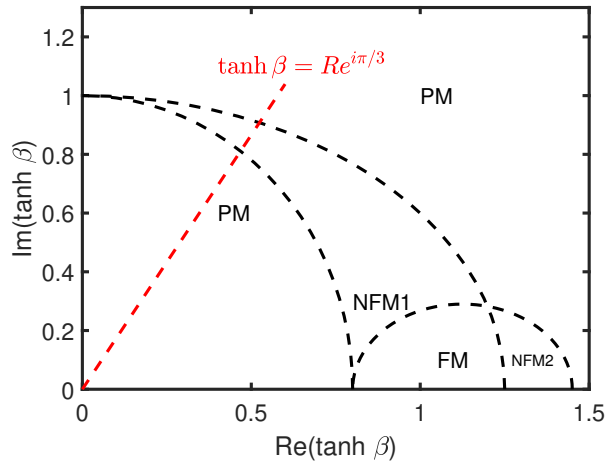


FIG. 1. Phase diagram of different spatial/temporal order of our quantum circuits. PM (paramagnet): short-range temporal and spatial order. FM (ferromagnet): long-range temporal and spatial order. NFM1 (non-ferromagnet 1): quasi-long-range temporal order. NFM2 (non-ferromagnet 2): quasi-long-range spatial order. Adapted from [18].

where N is number of Floquet steps and the choice of initial state ρ_0 is arbitrary for late-time behavior because non-Hermitian time evolution drives the system to a steady state. We therefore choose $\rho_0 \propto I$. We can also define two point spatial correlation function:

$$C(y) = \langle Z_{\frac{L}{2}-y} Z_{\frac{L}{2}+y} \rangle_{t \rightarrow \infty} \quad (4)$$

whose expectation value is evaluated in the steady state

$$|\psi(\infty)\rangle \propto \lim_{N \rightarrow \infty} \mathcal{U}^N |\psi(0)\rangle. \quad (5)$$

In the paramagnetic phase, both spatial and temporal correlations decay exponentially, $C(N) \sim e^{-N/\tau}$ and $C(y) \sim e^{-y/\xi}$, where $1/\tau$ and $1/\xi$ are (generally unequal) rates of temporal and spatial decays, respectively. In the time-crystalline (NFM1) phase, we expect[18] quasi-long-range-ordered oscillations, $C(N) \sim N^{-\alpha_1} \cos(a_1 N)$ where a_1 is a tunable oscillation frequency, while $C(y) \sim y^{-\alpha'_1}$. Spatial power-law decay has been documented[18] but the precise variation of time (space) exponents α_1 (α'_1) has not been understood in detail. Similarly, for the NFM2 phase, $C(y) \sim y^{-\alpha_2} \cos(a_2 y)$. For the ferromagnetic phase, $C(N)$ and $C(y)$ converge to a non-zero values at large N or y .

A. Interaction term

The Hermitian transverse-field Ising model is integrable. This is most readily seen by performing a Jordan-Wigner transformation to free Majorana fermions [31].

For non-Hermitian models, particularly those with time-dependence, the notion of free Majoranas is more complicated; for instance, adding disorder to the field or interaction terms makes the model much harder to solve. However, as discussed in [18], the notion of free fermion integrability remains when the system is translation-invariant.

In this paper, we add an interaction term $K \sum_j X_j X_{j+1}$. In the language of Majorana fermions, this is a four-fermion interaction. It is known to render the system non-integrable. The Floquet operator becomes

$$\mathcal{U}_{\text{total}} = \exp \left[\gamma \sum_j X_j + \overbrace{\gamma K \sum_j X_j X_{j+1}}^{\text{interaction}} \right] \times \exp \left[\sum_j J Z_j Z_{j+1} \right]. \quad (6)$$

Since this model is non-integrable, we are forced to resort to approximate methods for solving it. In particular, we consider mean-field theory, exact diagonalization, and time-evolving block decimation (TEBD); details are described below.

B. TEBD simulations of correlation function

The structure of non-Hermitian Floquet operators is relatively simple to implement with TEBD, as each term in $\mathcal{U}_{\text{total}}$ can be written as a product of local matrix product operators with small bond dimensions. In order to simulate the interacting model using TEBD, we use the python package TeNPy [32]. Non-Hermitian time evolution is obtained by decomposing each term into a Hermitian piece, which is done via conventional TEBD, and an anti-Hermitian piece, which is done via TEBD-like imaginary time evolution. A key challenge in practice is to obtain the two-time correlation function $C(N)$. We accomplished this via direct sampling of the infinite-temperature trace in terms of z -basis eigenstates.

To see how this works, let us rewrite the correlation function in terms of basis states $|\psi_\mu\rangle$:

$$C(N) = \frac{\sum_\mu \langle \psi_\mu | Z_j \mathcal{U}^N Z_j \rho_0 (\mathcal{U}^\dagger)^N | \psi_\mu \rangle}{\sum_\nu \langle \psi_\nu | \mathcal{U}^N \rho_0 (\mathcal{U}^\dagger)^N | \psi_\nu \rangle}. \quad (7)$$

Noting that we work in the z -basis, $\langle \psi_\mu | Z_j = s_{\mu j} \langle \psi_\mu |$ with $s_{\mu j} = \pm 1$. Thus,

$$\begin{aligned} C(N) &= \frac{\sum_\mu s_{\mu j} \langle \psi_\mu | \mathcal{U}^N Z_j (\mathcal{U}^\dagger)^N | \psi_\mu \rangle}{\sum_\nu \langle \psi_\nu | \mathcal{U}^N (\mathcal{U}^\dagger)^N | \psi_\nu \rangle} \\ &\equiv \frac{\sum_\mu s_{\mu j} \langle \psi_\mu(N) | Z_j | \psi_\mu(N) \rangle}{\sum_\nu \langle \psi_\nu(N) | \psi_\nu(N) \rangle} \end{aligned} \quad (8)$$

The non-unitary evolution operator \mathcal{U} will make the denominator in eqn. 7 exponentially grow or decay depending on its largest magnitude eigenvalue, that is,

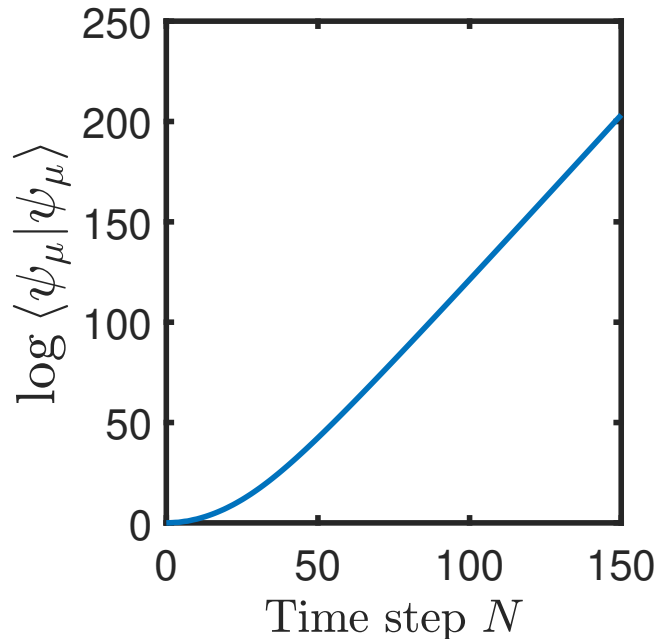


FIG. 2. Example fit of $\log \langle \psi_\mu | \psi_\mu \rangle \sim kN + \text{const}$ in NFM1 phase, averaged over initial states with $\tanh \beta = \exp(i\pi/3)$.

$\langle \psi(N) | \psi(N) \rangle \sim \exp(kN)$, which causes issues with numerical precision. To overcome this, we can fit the slope k as shown in in fig. 2 shift the Hamiltonians uniformly, $H \rightarrow H - k/2$. After the energy shifting, the denominator becomes smooth. Finally, the numerator and denominator are approximated by randomly sampling the initial states $|\psi_\mu\rangle$ and keeping track of their normalization during imaginary-time evolution.

A crucial point about the efficacy of these methods is that, unlike Hermitian time-evolution, the non-Hermitian evolution here naturally prevents an unbounded growth of the entanglement. Therefore, meaningful results are able to be obtained with moderate bond dimension, even for large time delay N . All data shown is converged in bond dimension; some illustrations are shown in the appendix B.

III. RESULTS

The non-Hermitian Floquet-Ising model described above is simulated using TEBD; results for two-time correlations in the PM phase and NFM1 phase are shown in Figure 3, both without integrability breaking ($K = 0$) and with integrability breaking ($K = 0.1$). In order to easily tune between the phases, throughout this section we take a cut in the complex $\tanh \beta$ plane given by

$$\tanh \beta = R e^{i\pi/3} \implies R = |\tanh \beta|, \quad (9)$$

as shown in Figure 1. The point $R = 1$, which lies in the middle of the NFM1 phase, is special because it corre-

sponds to a purely real (Hermitian) magnetic field term. Tuning away from this point, the PM phase is achieved upon either increasing or decreasing R by a sufficient amount.

Beginning with the PM phase, the correlations clearly decay exponentially in both cases, but the decay rate is modified by adding K . Furthermore, the decay rate increases with increasing K for $R = 0.7$, while decreasing with increasing K for $R = 1.3$. This suggests that the phase transition point – where decay rate goes to zero – is shifting further from the $R = 0.7$ point and closer to the $R = 1.3$ point.

In the NFM1 phase, the conclusion is less clear. The results are consistent with long-lived oscillations with a power-law envelope, but finite size effects prevent us from definitively establishing this numerically. Note that this is a limitation of TEBD not non-integrability, as a clear power law decay for $K = 0$ is also hard to establish. Therefore, in order to draw a clearer conclusion, we seek out alternative observables.

We find that a useful observable for disentangling this physics is the expectation value of the transverse magnetization X in the steady state, where $X \equiv L^{-1} \sum_j X_j$. As a leading approximation, in the paramagnetic (PM) phase, Z - Z correlations decay rapidly, suggesting that the Ising interaction is irrelevant. The dominant remaining term is a complex transverse field term, which in isolation leads to $\langle X \rangle$ values of 1 or -1 . In contrast, in the NFM1 phase, where the Z - Z correlation function exhibits persistent oscillations, $\langle X \rangle$ should fall within the range $[-1, 1]$. For the case $K = 0$, this behavior was seen in [18]; as we will see, it is also very useful for understanding the behavior of the model with $K > 0$.

We obtain $\langle X \rangle$ from TEBD by evolving the initial state to late times then calculating $\langle X \rangle$ in the steady state. The time evolution of $\langle X \rangle$ for a few different values of R is shown in fig. 4. Extracting the late-time $\langle X \rangle_{\text{ss}}$, we see that there are kinks at the two PM to NFM1 transitions for all values of K shown. As predicted from analyzing the two-time correlation functions, the phase boundary shifts upward to larger R values when $K > 0$ is added. However, we also see an unexpected new phenomenon, namely a jump in $\langle X \rangle_{\text{ss}}$ near $R = 1$. This jump is suggestive of a new first-order phase transition. We will now try to understand these two behaviors – shifting of the critical points and the new phase transition – using approximate treatments.

A. Mean-field treatment

As a first attempt, we notice that K is relatively small, suggesting to use a mean-field decoupling of the integrability-breaking interactions. Specifically, we ap-

proximate the interaction term by

$$\begin{aligned} \mathcal{K} &= \exp \left[K \gamma \sum_j X_j X_{j+1} \right] \\ &\approx \exp \left\{ \gamma K \sum_j X_j \int_0^1 dt \langle X(t) \rangle \right\} \\ &\quad \times \exp \left\{ -\gamma K \sum_j \int_0^1 dt \langle X(t) \rangle^2 \right\} . \end{aligned} \quad (10)$$

Furthermore, we assume that $\langle X(t) \rangle$ does not vary significantly over time, allowing us to approximate $\int_0^1 dt \langle X(t) \rangle = \langle X \rangle$ at the beginning of the non-unitary \mathcal{K} gate [33]. Therefore,

$$\mathcal{K} \approx \exp \left[2\gamma K \langle X \rangle \sum_j X_j \right] \exp \left[-2\gamma K L \langle X \rangle^2 \right] . \quad (11)$$

In Anderson pseudospin representation, we then solve [18]

$$\begin{aligned} \mathcal{W} &= \prod_{k>0} \exp \left[2J \left(\cos(k) \tau_k^z + \sin(k) \tau_k^y \right) \right] \\ \mathcal{V} &= \prod_{k>0} A^2(\gamma) \exp \left(2\gamma \tau_k^z \right) \\ \mathcal{K} &= \prod_{k>0} A^2(\gamma') \exp \left(2\gamma' \tau_k^z \right) \\ \mathcal{U} &= \mathcal{K} \mathcal{V}^{1/2} \mathcal{W} \mathcal{V}^{1/2} \equiv \prod_{k>0} \Theta_k \end{aligned} \quad (12)$$

where $\gamma' = 2\gamma K \langle X \rangle$ and $A(\gamma) = \sqrt{\coth \gamma - \tanh \gamma}$. Here we neglect the constant prefactor. Therefore,

$$\begin{aligned} \Theta_k &= A^2(\gamma) A^2(\gamma') \exp(\gamma \tau_k^z) \exp(2\gamma' \tau_k^z) \\ &\quad \times \exp \left[2J \left(\cos(k) \tau_k^z + \sin(k) \tau_k^y \right) \right] \exp(\gamma \tau_k^z) . \end{aligned} \quad (13)$$

These mean-field equations are challenging to solve analytically, but can be done numerically as follows. We know that $\langle X \rangle$ lies within the interval $[-1, 1]$. Therefore, we initially guess a value $\langle X \rangle_{\text{guess}}$ from this range. Next, we solve for the steady state and compute the corresponding $\langle X \rangle_{\text{actual}}$. We then iterate until these values match.

The mean-field values of $\langle X \rangle_{\text{ss}}$ are compared to the exact values in Figure 5. The shifts of the phase diagram are accurately captured by the this mean-field treatment at small and moderate K , meaning that this physics is just described by a self-consistent shift of the (complex) transverse field. Note that this works despite known issues with mean-field theory in one dimension because the remaining parts of the model are treated exactly via free fermions; the fluctuations missed by mean-field theory are irrelevant to shifts of the PM-NFM1 phase boundaries. However, this mean-field treatment completely misses the jump at $R = 1$.

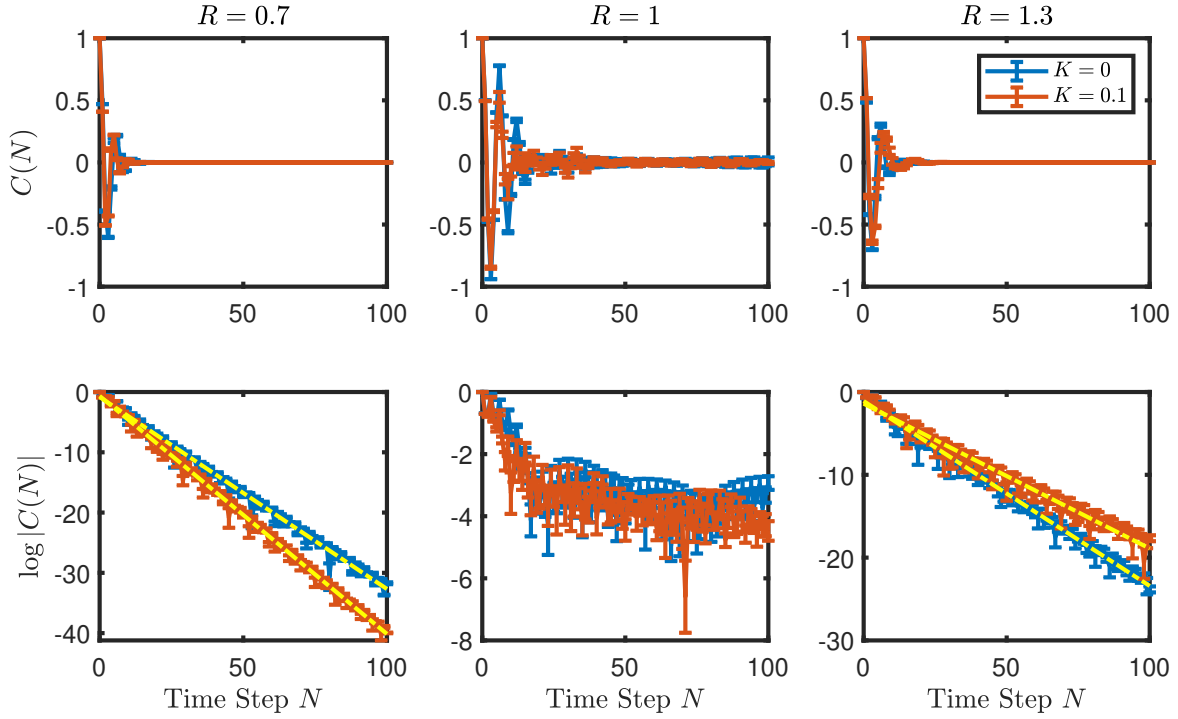


FIG. 3. Upper panels are two-time correlation function, and lower panels are logarithm of the magnitude of the two-time correlation function with $\tanh \beta = R \exp(i\pi/3)$. Left panels and right panels represent PM phase, and middle panels represent NFM1 phase. The blue curve represents the data without the interaction term, while the red curve includes the interaction term. The yellow dashed lines indicate linear fits to the data. The parameters used are system size $L = 150$, bond dimension $\chi = 60$.

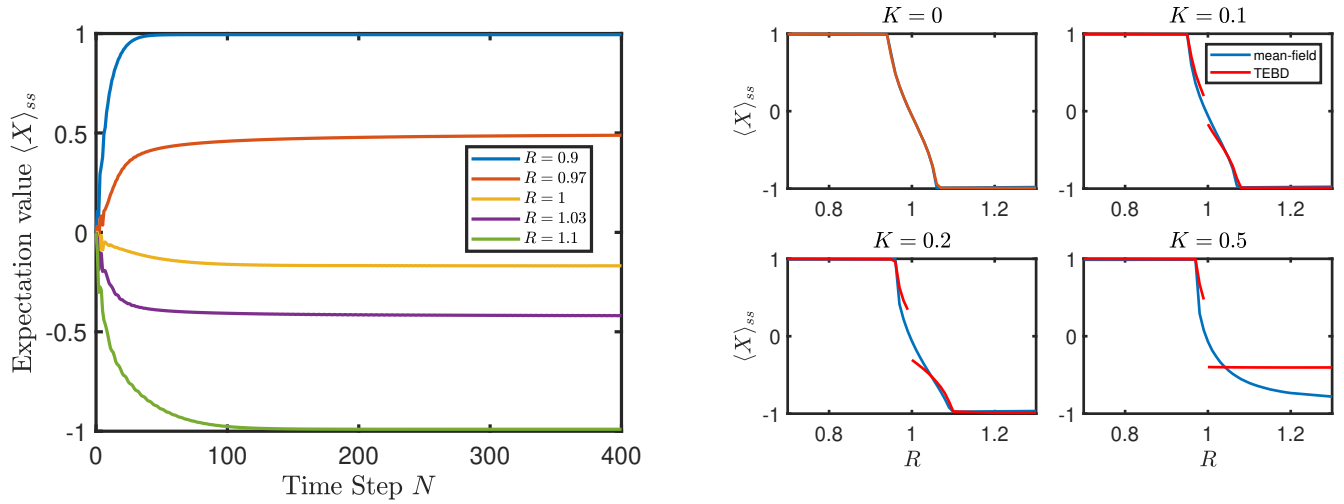


FIG. 4. The expectation value of X in the steady states. The parameters used are system size $L = 50$, $K = 0.1$, and $\tanh \beta = R \exp(i\pi/3)$.

FIG. 5. Expectation value from mean-field treatment with different K value, where $\tanh \beta = R \exp(i\pi/3)$. The panels are arranged as follows: upper left: $K = 0$, upper right: $K = 0.1$, lower left: $K = 0.2$, and lower right: $K = 0.5$.

B. Interaction-induced symmetry-breaking transition

In order to understand the jump at $R = 1$, we have found an average Hamiltonian treatment to be very valuable. Note first that $R = 1$ corresponds to purely imaginary transverse field $\gamma = -i\frac{\theta}{2} \equiv \gamma_0$, where $\theta = \arg[\tanh\beta]$ is chosen to be $\pi/3$ in all numerics. Meanwhile, both J and K are relatively small, so we consider J , K and $\Delta\gamma \equiv \gamma - \gamma_0$ as weak perturbations. (Appendix A) Then, as shown in A, we can go to a rotating frame corresponding to the field term γ_0 , and then time-average the remaining small terms to get the zeroth order ‘‘Floquet Hamiltonian’’

$$H_{\text{eff}} \approx i \sum_j \left(\Delta\gamma X_j + \gamma K X_j X_{j+1} + \frac{1}{2} J Z_j Z_{j+1} + \frac{1}{2} J Y_j Y_{j+1} \right) . \quad (14)$$

While this is derived for θ which is a rational multiple of π , for which a finite power of \mathcal{U}_0 gives the identity (here the 6th power because $6 \times (\pi/3) = 2\pi$), an equivalent expression holds for the average Hamiltonian in cases with irrational angles.

The Hamiltonian in Eq. 14 is a non-Hermitian XXZ model with quantization axis along x and a complex chemical potential term proportional to $\Delta\gamma$. For $\Delta\gamma = 0$, i.e., $R = 1$, one expects an XXZ model at half-filling, which has been extensively studied in both the Hermitian [34, 35] and non-Hermitian [36] case. In the easy-plane limit, $|J| \gg |\gamma K|$, one expects Luttinger liquid behavior; this has been shown even for the non-Hermitian case using Bethe ansatz and bosonization [36]. In the easy-axis limit, $|J| \ll |\gamma K|$, one expects Ising symmetry breaking along the quantization axis x . Finally, for $R \neq 1$ (i.e., $\Delta\gamma \neq 0$), the chemical potential pushes the steady state away from half-filling and gives a non-symmetry-broken state that is adiabatically connected to the Luttinger liquid. In the language of our non-Hermitian Floquet model, the non-interacting case $K = 0$ is precisely an easy-plane magnet. In other words, the Luttinger liquid phase in this rotating frame is equivalent to the time crystal (NFM1) phase in the lab frame. Finally, if the chemical potential strength $|\Delta\gamma|$ becomes sufficiently large, the states become either fully filled ($\langle X \rangle = 1$) or fully empty ($\langle X \rangle = -1$), which signifies a transition to the PM seen in our numerics.

The phase structure described above is completely consistent with what is seen in the exact numerics, despite the fact that it relies on having sufficiently small J , K , and $\Delta\gamma$ that higher-order terms in the Floquet expansion can be neglected (see Sec. A for more details). To demonstrate its validity, we compare $\langle X \rangle_{\text{ss}}$ obtained using TEBD to that of the steady state in H_{eff} in Fig. 6. Both clearly exhibit a jump near $R = 1$. The minor differences between the two curves can be attributed to the exclusion of higher orders of perturbation in our analysis, i.e., finite values of J and K .

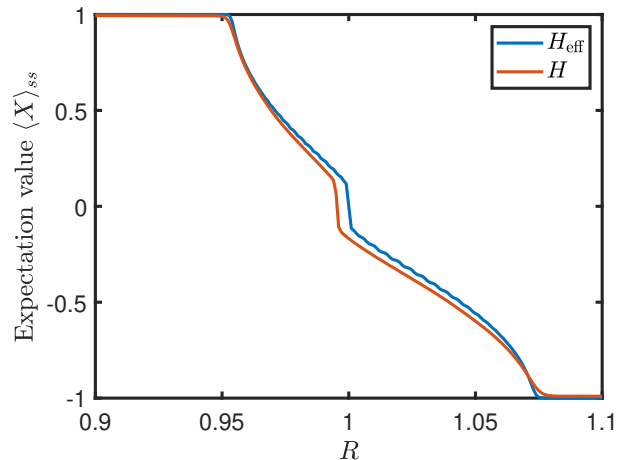


FIG. 6. Expectation value from H_{eff} and H with $\tanh\beta = R \exp(i\pi/3)$ and $K = 0.1$.

Next, to identify the critical point of this transition, we look in the limit $|\Delta\gamma| \rightarrow 0$ very near $R = 1$. Specifically, we choose $R = 0.9998$ where $\text{Re}(\Delta\gamma) = 0.0001$, and $R = 1.0002$ where $\text{Re}(\Delta\gamma) = -0.0001$ as illustrated in fig. 7. The magnetization shows a clear Luttinger liquid to x -ferromagnet transition at $K_c \approx 0.085$. This confirms that the phase structure of H_{eff} is imprinted on that of the full interacting Floquet circuit.

Combine the results from above, the phase diagram of our model as illustrated in Fig. 8. Crucially, as our initial data indicated, we predict that the Luttinger liquid / NFM1 phase survives in the presence of finite K , even for $K > K_c$, based on the known stability of the Luttinger liquid to weak integrability breaking terms – here given by higher-order corrections to H_{eff} . Finally, we identify the new phase of matter at $R = 1$ and $K > K_c$ as an x -ferromagnetic in the rotating frame which can be described by the easy-axis limit of the non-Hermitian XXZ model. Note that this is completely different than the z -ferromagnet that exists in the model for $K = 0$; our integrability-breaking perturbation is vital for realizing this new phase.

IV. DISCUSSION

We introduce a non-integrable interaction term to the non-Hermitian Floquet transverse-field Ising model, calculate the correlation function, and observe that this interaction term induces a shift in the phase diagram. A mean-field treatment is employed to analytically interpret the effect of the interaction term, confirming the observed shift. Additionally, the numerical TEBD data reveals an extra symmetry breaking that is absent in the mean-field treatment. To further investigate this, we use a variant of the Floquet high-frequency expansion to derive an effective Hamiltonian, which corrobo-

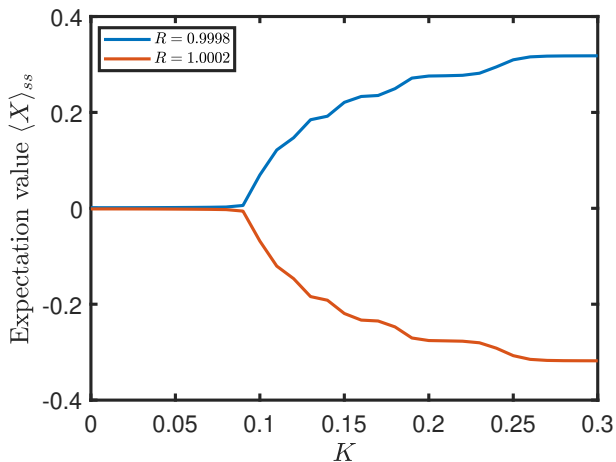


FIG. 7. Expectation value from H_{eff} . $\tanh\beta = \exp(i\pi/3)$. $R = 0.9998$ where $\text{Re}(\Delta\gamma) = 0.0001$, and $R = 1.0002$ where $\text{Re}(\Delta\gamma) = -0.0001$. We can determine the critical point as $K_c \approx 0.085$. For $K < K_c$, there is no observable jump; for $K > K_c$, the magnitude of the jump increases with an increase in K .

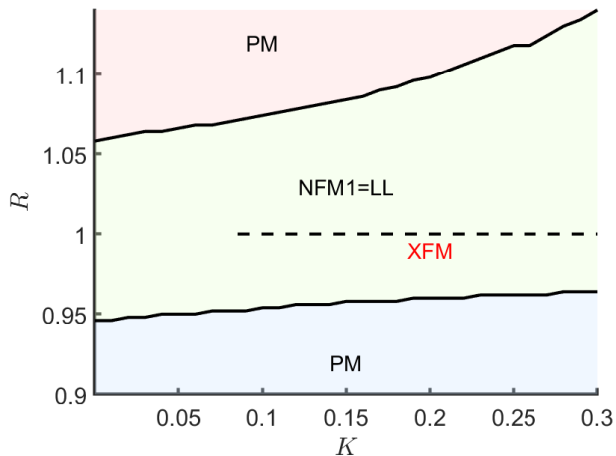


FIG. 8. Phase diagram after adding interaction term. $\tanh\beta = \exp(i\pi/3)$. Two solid black lines are the boundary between PM phase and NFM1 phase. The dashed line is the additional symmetry breaking (XFM phase). The critical point is $K_c \approx 0.085$. For $K < K_c$, there is no observable jump.

rates the additional symmetry breaking as coming from

a non-Hermitian XXZ Hamiltonian. These predictions are consistent with exact TEBD numerics, and similar methods are likely to allow study of other phases in this model (e.g., for $\arg[\tanh\beta] \neq \pi/3$) and perhaps for other non-Hermitian models.

Based on the XXZ analysis, we predict that this phase structure will be quite stable, for example to the addition of other weak symmetry-respecting perturbations including those found at higher order in the Floquet expansion. This argument relies on the fact that an effective non-Hermitian Hamiltonian exists for which we expect the steady state to be quite similar to the ground state of a conventional Hermitian Hamiltonian. Therefore, for example, one should obtain conventional XXZ criticality in the vicinity of K_c , although the correlation functions may pick up damping factors similar to those obtained when considering complex-time correlation functions in the vicinity of a conventional quantum critical point. An intriguing open question is whether the phase boundary should in fact remain smooth as a function of $\theta = \arg[\tanh\beta]$, given that the Floquet expansion relied on a rational multiple of π to define a finite super-Floquet cycle. One potential solution for irrational angles is to consider a nearby low-denominator rational, and then treat deviations of the angle from this rational approximation as part of $\Delta\gamma$. It remains unclear whether this analysis would give rise to a smooth phase boundary, or whether the structure of the irrational numbers would give rise to a punctured (fractal?) phase boundary as has been seen in other quasiperiodically driven systems [37]. More broadly, the unexpected symmetry breaking that we observe emphasizes the rich physics that emerges from the interplay between non-Hermitian effects and many-body interactions. These findings may have important implications for more general phase structure of driven non-Hermitian systems, an increasingly active field whose properties are increasingly able to be studied in controllable quantum systems where the desired interactions and non-Hermitian dynamics can be engineered [38].

ACKNOWLEDGMENTS

Work was performed with support from the National Science Foundation through award number DMR-1945529 (MK) and the Welch Foundation through award number AT-2036-20200401 (MK and WX).

Appendix A: Effective Hamiltonian by weak perturbation

In this appendix, we derive the effective Hamiltonian using a Floquet high-frequency expansion. Let's start by considering Floquet perturbation theory around the point with $\tanh\beta = e^{i\theta}$ for $\theta = \pi/3$ and with $J = 0$. This corresponds to $\gamma = -i\theta/2 = -i\pi/6 \equiv \gamma_0$. Then J , K , and deviations of γ from this fine-tuned point will be treated as weak perturbations. Applying this idea directly to the period-6 time-evolution operator \mathcal{U}^6 . Specifically, we will

break it up as follows:

$$\mathcal{U} = \mathcal{U}_x \mathcal{U}_{zz} \tag{A1}$$

$$\mathcal{U}_x = \exp \left[\gamma \left(\sum_j (X_j + K X_j X_{j+1}) \right) \right] \tag{A2}$$

$$\mathcal{U}_{zz} = \exp \left[J \sum_j Z_j Z_{j+1} \right] \tag{A3}$$

Define the case with $J = K = \Delta\gamma = 0$ as \mathcal{U}_0 (where $\Delta\gamma \equiv \gamma - \gamma_0$). Then first note that

$$\mathcal{U}_0^6 = e^{6\gamma_0 \sum_j X_j} = \prod_j e^{-i\pi X_j} \propto 1. \tag{A4}$$

Now, to perturb around this point, we go into a rotating frame as follows:

$$\mathcal{U}^6 = \mathcal{U}_x \mathcal{U}_{zz} \mathcal{U}_x \mathcal{U}_{zz} \mathcal{U}_x \mathcal{U}_{zz} \mathcal{U}_x \mathcal{U}_{zz} \mathcal{U}_x \mathcal{U}_{zz} \mathcal{U}_x \mathcal{U}_{zz} \tag{A5}$$

$$= \mathcal{U}_0 \mathcal{U}_{\Delta x} \mathcal{U}_{zz} \mathcal{U}_0 \mathcal{U}_{\Delta x} \mathcal{U}_{zz} \mathcal{U}_0 \mathcal{U}_{\Delta x} \mathcal{U}_{zz} \mathcal{U}_0 \mathcal{U}_{\Delta x} \mathcal{U}_{zz} \mathcal{U}_0 \mathcal{U}_{\Delta x} \mathcal{U}_{zz} \mathcal{U}_0 \mathcal{U}_{\Delta x} \mathcal{U}_{zz} \tag{A6}$$

$$= \mathcal{U}_0^6 \mathcal{U}_{\Delta x} (\mathcal{U}_0^\dagger)^5 \mathcal{U}_{zz} \mathcal{U}_0^5 \mathcal{U}_{\Delta x} (\mathcal{U}_0^\dagger)^4 \mathcal{U}_{zz} \mathcal{U}_0^4 \mathcal{U}_{\Delta x} (\mathcal{U}_0^\dagger)^3 \mathcal{U}_{zz} \mathcal{U}_0^3 \mathcal{U}_{\Delta x} (\mathcal{U}_0^\dagger)^2 \mathcal{U}_{zz} \mathcal{U}_0^2 \mathcal{U}_{\Delta x} \mathcal{U}_0^\dagger \mathcal{U}_{zz} \mathcal{U}_0 \mathcal{U}_{\Delta x} \mathcal{U}_{zz} \tag{A7}$$

where we used that

$$\mathcal{U}_{\Delta x} \equiv \exp \left[\sum_j (\Delta\gamma X_j + \gamma K X_j X_{j+1}) \right] \tag{A8}$$

commutes with \mathcal{U}_0 . We recognize two of the terms as Heisenberg picture representations of the ZZ -interactions, allowing us to rewrite as

$$\mathcal{U}_0^\dagger \mathcal{U}_{zz} \mathcal{U}_0 = \exp \left[J \sum_j \mathcal{U}_0^\dagger Z_j \mathcal{U}_0 \mathcal{U}_0^\dagger Z_{j+1} \mathcal{U}_0 \right] \tag{A9}$$

$$\mathcal{U}_0^\dagger Z \mathcal{U}_0 = e^{i\pi X/6} Z e^{-i\pi X/6} = \frac{1}{2} Z + \frac{\sqrt{3}}{2} Y \tag{A10}$$

$$(\mathcal{U}_0^\dagger)^2 Z \mathcal{U}_0^2 = -\frac{1}{2} Z + \frac{\sqrt{3}}{2} Y \tag{A11}$$

$$(\mathcal{U}_0^\dagger)^3 Z \mathcal{U}_0^3 = -Z \tag{A12}$$

$$(\mathcal{U}_0^\dagger)^4 Z \mathcal{U}_0^4 = -\frac{1}{2} Z - \frac{\sqrt{3}}{2} Y \tag{A13}$$

$$(\mathcal{U}_0^\dagger)^5 Z \mathcal{U}_0^5 = \frac{1}{2} Z - \frac{\sqrt{3}}{2} Y \tag{A14}$$

$$\mathcal{U}_0^\dagger \mathcal{U}_{zz} \mathcal{U}_0 = \exp \left[\frac{J}{4} \sum_j (Z_j + \sqrt{3} Y_j) (Z_{j+1} + \sqrt{3} Y_{j+1}) \right] \tag{A15}$$

$$= \exp \left[\frac{J}{4} \sum_j (Z_j Z_{j+1} + \sqrt{3} Y_j Z_{j+1} + \sqrt{3} Z_j Y_{j+1} + 3 Y_j Y_{j+1}) \right] \tag{A16}$$

$$(\mathcal{U}_0^\dagger)^2 \mathcal{U}_{zz} \mathcal{U}_0^2 = \exp \left[\frac{J}{4} \sum_j (Z_j Z_{j+1} - \sqrt{3} Y_j Z_{j+1} - \sqrt{3} Z_j Y_{j+1} + 3 Y_j Y_{j+1}) \right] \tag{A17}$$

$$(\mathcal{U}_0^\dagger)^3 \mathcal{U}_{zz} \mathcal{U}_0^3 = \exp \left[\frac{J}{4} \sum_j (4 Z_j Z_{j+1}) \right] \tag{A18}$$

$$(\mathcal{U}_0^\dagger)^4 \mathcal{U}_{zz} \mathcal{U}_0^4 = \exp \left[\frac{J}{4} \sum_j (Z_j Z_{j+1} + \sqrt{3} Y_j Z_{j+1} + \sqrt{3} Z_j Y_{j+1} + 3 Y_j Y_{j+1}) \right] \tag{A19}$$

$$(\mathcal{U}_0^\dagger)^5 \mathcal{U}_{zz} \mathcal{U}_0^5 = \exp \left[\frac{J}{4} \sum_j (Z_j Z_{j+1} - \sqrt{3} Y_j Z_{j+1} - \sqrt{3} Z_j Y_{j+1} + 3 Y_j Y_{j+1}) \right] \tag{A20}$$

Putting it together, we have

$$\mathcal{U}^6 = \exp \left[\sum_j (\Delta\gamma X_j + \gamma K X_j X_{j+1}) \right] \exp \left[\frac{J}{4} \sum_j (Z_j Z_{j+1} - \sqrt{3} Y_j Z_{j+1} - \sqrt{3} Z_j Y_{j+1} + 3 Y_j Y_{j+1}) \right] \times \quad (\text{A21})$$

$$\exp \left[\sum_j (\Delta\gamma X_j + \gamma K X_j X_{j+1}) \right] \exp \left[\frac{J}{4} \sum_j (Z_j Z_{j+1} + \sqrt{3} Y_j Z_{j+1} + \sqrt{3} Z_j Y_{j+1} + 3 Y_j Y_{j+1}) \right] \times \quad (\text{A22})$$

$$\exp \left[\sum_j (\Delta\gamma X_j + \gamma K X_j X_{j+1}) \right] \exp \left[J \sum_j Z_j Z_{j+1} \right] \times \quad (\text{A23})$$

$$\exp \left[\sum_j (\Delta\gamma X_j + \gamma K X_j X_{j+1}) \right] \exp \left[\frac{J}{4} \sum_j (Z_j Z_{j+1} - \sqrt{3} Y_j Z_{j+1} - \sqrt{3} Z_j Y_{j+1} + 3 Y_j Y_{j+1}) \right] \times \quad (\text{A24})$$

$$\exp \left[\sum_j (\Delta\gamma X_j + \gamma K X_j X_{j+1}) \right] \exp \left[\frac{J}{4} \sum_j (Z_j Z_{j+1} + \sqrt{3} Y_j Z_{j+1} + \sqrt{3} Z_j Y_{j+1} + 3 Y_j Y_{j+1}) \right] \times \quad (\text{A25})$$

$$\exp \left[\sum_j (\Delta\gamma X_j + \gamma K X_j X_{j+1}) \right] \exp \left[J \sum_j Z_j Z_{j+1} \right] \quad (\text{A26})$$

Then, since there are no ‘‘large’’ terms left, we can think of this is the time evolution for time $T = 6$ (in units of the original Floquet cycle) of an effective Hamiltonian, such that

$$\mathcal{U}^6 = e^{-6iH_{\text{eff}}} \implies H_{\text{eff}} = \frac{i}{6} \ln(\mathcal{U}^6). \quad (\text{A27})$$

Assuming $|\Delta\gamma|$, $|K|$, and $|J|$ are all much less than π , we can get an expression for H_{eff} order-by-order using Baker-Campbell-Hausdorff. At leading order, the result is just the average Hamiltonian.

$$H_{\text{eff}} \approx \frac{i}{6} \left[6 \sum_j (\Delta\gamma X_j + \gamma K X_j X_{j+1}) + 3J \sum_j (Z_j Z_{j+1} + Y_j Y_{j+1}) \right] \quad (\text{A28})$$

$$= i \sum_j \left(\Delta\gamma X_j + \gamma K X_j X_{j+1} + \frac{1}{2} J Z_j Z_{j+1} + \frac{1}{2} J Y_j Y_{j+1} \right). \quad (\text{A29})$$

To make the Floquet operator more symmetric, we choose $\mathcal{U} = \mathcal{U}_x^{\frac{1}{2}} \mathcal{U}_z \mathcal{U}_x^{\frac{1}{2}}$ and considering a simple case $\tanh \beta = \exp(i\frac{2\pi}{3})$, $\gamma_0 = -\frac{i\pi}{3}$.

$$\mathcal{U}^3 = \mathcal{U}_x^{\frac{1}{2}} \mathcal{U}_z \mathcal{U}_x^{\frac{1}{2}} \mathcal{U}_x^{\frac{1}{2}} \mathcal{U}_z \mathcal{U}_x^{\frac{1}{2}} \mathcal{U}_x^{\frac{1}{2}} \mathcal{U}_z \mathcal{U}_x^{\frac{1}{2}} \quad (\text{A30})$$

$$= \mathcal{U}_0^{\frac{6}{2}} \mathcal{U}_{\Delta x}^{\frac{1}{2}} (\mathcal{U}_0^\dagger)^{\frac{5}{2}} \mathcal{U}_{zz} \mathcal{U}_0^{\frac{5}{2}} \mathcal{U}_{\Delta x} (\mathcal{U}_0^\dagger)^{\frac{3}{2}} \mathcal{U}_{zz} \mathcal{U}_0^{\frac{3}{2}} \mathcal{U}_{\Delta x} (\mathcal{U}_0^\dagger)^{\frac{1}{2}} \mathcal{U}_{zz} \mathcal{U}_0^{\frac{1}{2}} \mathcal{U}_{\Delta x} \quad (\text{A31})$$

$$= \exp \left[\frac{1}{2} \sum_j (\Delta\gamma X_j + \gamma K X_j X_{j+1}) \right] \exp \left[\frac{J}{4} \sum_j (Z_j Z_{j+1} - \sqrt{3} Y_j Z_{j+1} - \sqrt{3} Z_j Y_{j+1} + 3 Y_j Y_{j+1}) \right] \times \quad (\text{A32})$$

$$\exp \left[\sum_j (\Delta\gamma X_j + \gamma K X_j X_{j+1}) \right] \exp \left[\frac{J}{4} \sum_j (4 Z_j Z_{j+1}) \right] \times \quad (\text{A33})$$

$$\exp \left[\sum_j (\Delta\gamma X_j + \gamma K X_j X_{j+1}) \right] \exp \left[\frac{J}{4} \sum_j (Z_j Z_{j+1} + \sqrt{3} Y_j Z_{j+1} + \sqrt{3} Z_j Y_{j+1} + 3 Y_j Y_{j+1}) \right] \times \quad (\text{A34})$$

$$\exp \left[\frac{1}{2} \sum_j (\Delta\gamma X_j + \gamma K X_j X_{j+1}) \right] \quad (\text{A35})$$

Similarly,

$$H_{\text{eff}} \approx \frac{i}{3} \left[3 \sum_j (\Delta\gamma X_j + \gamma K X_j X_{j+1}) + \frac{3}{2} J \sum_j (Z_j Z_{j+1} + Y_j Y_{j+1}) \right] \quad (\text{A36})$$

$$= i \sum_j \left(\Delta\gamma X_j + \gamma K X_j X_{j+1} + \frac{1}{2} J Z_j Z_{j+1} + \frac{1}{2} J Y_j Y_{j+1} \right). \quad (\text{A37})$$

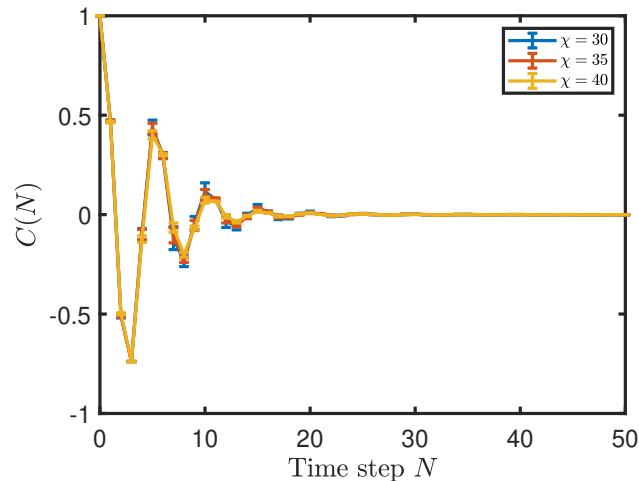


FIG. 9. Example of convergence with bond dimension in PM phase with $K = 0.1$, $\tanh \beta = 0.8 \exp(i\pi/3)$.

Appendix B: Convergence with bond dimension

All data shown in this paper are converged in bond dimension, Figure 9 is an example.

-
- [1] D. Manzano, A short introduction to the lindblad master equation, *AIP Advances* **10**, 025106 (2020).
- [2] M. Naghiloo, M. Abbasi, Y. N. Joglekar, and K. W. Murch, Quantum state tomography across the exceptional point in a single dissipative qubit, *Nature Physics* **15**, 1232 (2019).
- [3] E. J. Bergholtz, J. C. Budich, and F. K. Kunst, Exceptional topology of non-hermitian systems, *Rev. Mod. Phys.* **93**, 015005 (2021).
- [4] S. Yao and Z. Wang, Edge states and topological invariants of non-hermitian systems, *Phys. Rev. Lett.* **121**, 086803 (2018).
- [5] X.-D. Cui and Y. Zheng, Geometric phases in non-hermitian quantum mechanics, *Phys. Rev. A* **86**, 064104 (2012).
- [6] J. Doppler, A. A. Mailybaev, J. Böhm, U. Kuhl, A. Girschik, F. Libisch, T. J. Milburn, P. Rabl, N. Moiseyev, and S. Rotter, Dynamically encircling an exceptional point for asymmetric mode switching, *Nature* **537**, 76 (2016).
- [7] H. Xu, D. Mason, L. Jiang, and J. G. E. Harris, Topological energy transfer in an optomechanical system with exceptional points, *Nature* **537**, 80 (2016).
- [8] L. Guo, L. Du, C. Yin, Y. Zhang, and S. Chen, Dynamical evolutions in non-hermitian triple-well systems with a complex potential, *Phys. Rev. A* **97**, 032109 (2018).
- [9] C. M. Bender, D. C. Brody, and H. F. Jones, Complex extension of quantum mechanics, *Phys. Rev. Lett.* **89**, 270401 (2002).
- [10] M. V. Berry, Optical polarization evolution near a non-hermitian degeneracy, *Journal of Optics* **13**, 115701 (2011).
- [11] S. Longhi, Bloch oscillations in complex crystals with \mathcal{PT} symmetry, *Phys. Rev. Lett.* **103**, 123601 (2009).
- [12] C. T. West, T. Kottos, and T. c. v. Prosen, \mathcal{PT} -symmetric wave chaos, *Phys. Rev. Lett.* **104**, 054102 (2010).
- [13] C. E. Rüter, K. G. Makris, R. El-Ganainy, D. N. Christodoulides, M. Segev, and D. Kip, Observation of parity-time symmetry in optics, *Nature Physics* **6**, 192 (2010).
- [14] J. Li, A. K. Harter, J. Liu, L. de Melo, Y. N. Joglekar, and L. Luo, Observation of parity-time symmetry breaking transitions in a dissipative floquet system of ultracold atoms, *Nature Communications* **10**, 855 (2019).
- [15] M.-A. Miri and A. Alù, Exceptional points in optics and photonics, *Science* **363**, eaar7709 (2019), <https://www.science.org/doi/pdf/10.1126/science.aar7709>.
- [16] T. Gao, E. Estrecho, K. Y. Bliokh, T. C. H. Liew, M. D. Fraser, S. Brodbeck, M. Kamp, C. Schneider, S. Höfling, Y. Yamamoto, F. Nori, Y. S. Kivshar, A. G. Truscott, R. G. Dall, and E. A. Ostrovskaya, Observation of non-hermitian degeneracies in a chaotic exciton-polariton billiard, *Nature* **526**, 554 (2015).
- [17] D. Zhang, X.-Q. Luo, Y.-P. Wang, T.-F. Li, and J. Q. You, Observation of the exceptional point in cavity magnon-polaritons, *Nature Communications* **8**, 1368 (2017).
- [18] S. Basu, D. P. Arovas, S. Gopalakrishnan, C. A. Hooley, and V. Oganessian, Fisher zeros and persistent temporal oscillations in nonunitary quantum circuits, *Phys. Rev. Research* **4**, 013018 (2022).

- [19] C. N. Yang and T. D. Lee, Statistical theory of equations of state and phase transitions. i. theory of condensation, *Phys. Rev.* **87**, 404 (1952).
- [20] T. D. Lee and C. N. Yang, Statistical theory of equations of state and phase transitions. ii. lattice gas and ising model, *Phys. Rev.* **87**, 410 (1952).
- [21] R. B. Griffiths, Nonanalytic behavior above the critical point in a random ising ferromagnet, *Phys. Rev. Lett.* **23**, 17 (1969).
- [22] F. Wilczek, Quantum time crystals, *Phys. Rev. Lett.* **109**, 160401 (2012).
- [23] H. Watanabe and M. Oshikawa, Absence of quantum time crystals, *Phys. Rev. Lett.* **114**, 251603 (2015).
- [24] C. W. von Keyserlingk and S. L. Sondhi, Phase structure of one-dimensional interacting floquet systems. ii. symmetry-broken phases, *Phys. Rev. B* **93**, 245146 (2016).
- [25] D. V. Else, B. Bauer, and C. Nayak, Floquet time crystals, *Phys. Rev. Lett.* **117**, 090402 (2016).
- [26] J. Rovny, R. L. Blum, and S. E. Barrett, Observation of discrete-time-crystal signatures in an ordered dipolar many-body system, *Phys. Rev. Lett.* **120**, 180603 (2018).
- [27] S. Autti, V. B. Eltsov, and G. E. Volovik, Observation of a time quasicrystal and its transition to a superfluid time crystal, *Phys. Rev. Lett.* **120**, 215301 (2018).
- [28] S. Choi, J. Choi, R. Landig, G. Kucsko, H. Zhou, J. Isoya, F. Jelezko, S. Onoda, H. Sumiya, V. Khemani, C. von Keyserlingk, N. Y. Yao, E. Demler, and M. D. Lukin, Observation of discrete time-crystalline order in a disordered dipolar many-body system, *Nature* **543**, 221 (2017).
- [29] X. Mi, M. Ippoliti, C. Quintana, et al., Time-crystalline eigenstate order on a quantum processor, *Nature* **601**, 531 (2022).
- [30] V. Khemani, A. Lazarides, R. Moessner, and S. L. Sondhi, Phase structure of driven quantum systems, *Phys. Rev. Lett.* **116**, 250401 (2016).
- [31] S. Sachdev, Quantum Phase Transitions (Cambridge University Press, 2011).
- [32] J. Hauschild and F. Pollmann, Efficient numerical simulations with Tensor Networks: Tensor Network Python (TeNPy), *SciPost Phys. Lect. Notes* , 5 (2018).
- [33] While it may seem that $\langle X \rangle$ is conserved during time evolution, as it commutes with the XX -interacting Hamiltonian, this is not true for non-Hermitian time evolution because the different X -sectors can pick up different normalizations.
- [34] T. Sabetta and G. Misguich, Nonequilibrium steady states in the quantum xxz spin chain, *Phys. Rev. B* **88**, 245114 (2013).
- [35] D. Giuliano, D. Rossini, P. Sodano, and A. Trombettoni, Xxz spin- $\frac{1}{2}$ representation of a finite- u bose-hubbard chain at half-integer filling, *Phys. Rev. B* **87**, 035104 (2013).
- [36] K. Yamamoto, M. Nakagawa, M. Tezuka, M. Ueda, and N. Kawakami, Universal properties of dissipative tomonaga-luttinger liquids: Case study of a non-hermitian xxz spin chain, *Phys. Rev. B* **105**, 205125 (2022).
- [37] R. Artuso, P. Cvitanović, and B. G. Kenny, Phase transitions on strange irrational sets, *Phys. Rev. A* **39**, 268 (1989).
- [38] W. Xie, M. Kolodrubetz, and V. Oganesyan, Effect of noise on quantum circuit realization of non-hermitian time (2024), arXiv:2409.06113 [cond-mat.str-el].